XIV International Conference on Computational Plasticity. Fundamentals and Applications
COMPLAS 2019
E. Oñate, D.R.J. Owen, D. Peric , M. Chiumenti, and Eduardo de Souza Neto (Eds)

NEW APPROACH FOR DETERMINATION OF STRAIN RATE SENSITIVITY OF MILD STEEL DC01 UNDER STACK COMPRESSION AND UNIAXIAL TENSILE TESTS

PEDRAM FARAHNAK[1,2], MIROSLÁV URBANEK[1], MARTIN RUND[1], JAN DŽUGAN[1], STEFFEN GERKE[2] AND MICHAEL BRÜNIG[2]

[1] COMTES FHT a.s., Průmyslová 995, 33441, Dobřany, Czech Republic

[2] Institut für Mechanik und Statik, Universität der Bundeswehr München, Werner-Heisenberg-Weg 39, D-85577 Neubiberg, Germany

email: pfarahnak@comtesfht.cz, www.comtesfht.com

Key words: Material Characterization, Forming Process, Strain Rate Sensitivity, Tensile Test, Stack Compression Test

Abstract. Deformation under uniaxial tensile loading with using Digital Image Correlations (DIC) is the easiest way to analyze the material behavior in sheet metal forming. In order to determine the plastic parameters such as hardening, anisotropy and strain rate sensitivity at higher strain level, equi-biaxial stress state is prerequisite. As reported in the literature, Bulge tests are frequently used for this purpose, but in this work, stack compression test is used as an alternative. In this experiment, deformation in the middle layer where the friction effect is the lowest was monitored using two pairs of DIC systems in rolling and transversal directions. Uniaxial tensile tests as well as stack compression tests were performed on mild ferritic steel DC01 at different strain rates, from $0.001\ s^{-1}$ to $10\ s^{-1}$. Strain rate sensitivity parameter was investigated at different level of strains for both experiments and strain rate sensitivity profiles were obtained. Results show a decrease of material strain rate sensitivity with increasing the true strain.

1 INTRODUCTION

In sheet metal forming, the quality of the simulation results highly depends on the input data and material parameters. The aim of numerical simulation is to describe the real experiment as accurate as possible. The main parameters for the plastic material behaviour are the yield curve, Lankford ratio and strain rate sensitivity which can be determined by different tests like tensile, Bulge and compression tests. Material hardening is a function of work hardening, strain rate sensitivity and temperature. Since cold forming mainly depends on work hardening and strain rate sensitivity, therefore, the temperature is not considered in the presented paper. Tensile test in sheet metal forming is well-known and frequently used for determination of elastic and plastic parameters. Tensile tests are frictionless and strain rate can be controlled by the test velocity, however, only the uniaxial material behaviour can be described. Therefore, equi-biaxial stress state is prerequisite for determination of plastic parameters at higher strain level. Jocham et al [1] determined the strain rate sensitivity profile for DC06 through tensile and Bulge tests. The Bulge test is a well-known biaxial experiment

and it is standardized in ISO-16808 [2]. In this work, stack layer compression test is used as an alternative to show the material behaviour from strain rate $0.001\ s^{-1}$ to $10\ s^{-1}$.

The stack discs compression was proposed by Pawelski [3]. For stack compression test, a set of stacked discs must be arranged to obtain a correct alignment between the discs. This preserves the material orientations in the stacked discs. This experiment was mainly used to determine the biaxial Lankford ratio which is the division of strain in transversal direction to strain in rolling direction [4,5]. Merklein and Kuppert [6] proposed a method to determine the flow curve at high strain level from stack compression test by measuring the true area during the experiment. For this purpose, two pairs of DIC systems with angle $90°$ towards each other, capture the deformation in the middle layer and in rolling and transversal directions. It is worth noting that in the middle layer the friction effect is less due to the upper and lower disc layers. In this experiment, the extension of the true area can be calculated through two true principal strains, one in rolling and another in transversal directions. Subsequently, true stress can be calculated thanks to load cell and the obtained true area. Similar to Bulge test, it provides the plastic parameters at higher strain levels. Suttner and Merklein [7] performed bulge test on different materials and it was found that for some materials like aluminum and advanced high strength steels, the obtained flow curves are in close agreement with uniaxial flow curve, however, for mild steels the biaxial flow curve is different from uniaxial one and it has to be converted to uniaxial flow curve according to ISO-16808 [2]. In this work, stack compression tests are performed at different velocities for determination of plastic parameter at different strain rates.

Strain rate sensitivity describes the dynamic material behavior and is defined by the average slopes in the logarithmic space of true stress and strain rate. Many definitions are available for the strain rate sensitivity in the literature. Jump test provides the instantaneous value of strain rate sensitivity without consideration of strain path history [8]. The concept of dynamic factors, i.e. the ratio of dynamic to static yield stresses was used in [8, 9]. The strain rate sensitivity is denoted by m and calculated mainly in publications based on the strain rate dependency of flow curves [10-14] and it can be expressed in the form:

$$m = \frac{\partial log\sigma}{\partial log\dot{\varepsilon}} \tag{1}$$

Where σ is the true yield stress and $\dot{\varepsilon}$ is the strain rate.

In this work, the material under investigation is mild ferritic steel DC01 and Table 1 represents the chemical composition of the material. In this work, uniaxial tensile tests are performed at different velocities at which the strain rate varies from $0.001\ s^{-1}$ to $10\ s^{-1}$. On the other hand, stack compression tests are performed as well at the interested strain rate range to provide the plastic parameters at higher strain levels. Finally, results are discussed for mild steel DC01.

Table 1: Chemical composition of mild ferritic steel DC01

C [%]	Mn [%]	P [%]	S [%]
0.12	0.6	0.045	0.045

2 EXPERIMENTAL AND NUMERICAL RESULTS

2.1 Uniaxial tensile test

Figure 1 (a) and (b) depict the geometry of standard and non-standard dog-bone specimens, respectively and the sheet thickness is 1.5 mm. Throughout this paper, all the dimensions are presented in terms of mm. Standard specimen is used for static test with strain rate $0.001\ s^{-1}$, while non-standard one for dynamic tests with strain rates 0.1 and $10\ s^{-1}$.

For static test, electro-mechanical testing system, Mayes, is used to conduct the uniaxial tests and the GOM Aramis^{TM} system with a 4 megapixel camera is utilized to monitor $2D$ strain fields with high resolution. The data acquisition rate is set at $100\ Hz$ in the testing system for accurate measuring of the tensile behaviour. For evaluation of the experiments, initial length of extensometers is chosen as $80\ mm$. Farahnak et al [15-17] performed other tensile tests on standard and miniature samples in transversal and diagonal directions to investigate about anisotropic behaviour of the material and it was observed that engineering stress-strain curves as well as Lankford ratios are very close to each other. Therefore, throughout this paper the material is assumed as an isotropic material for numerical simulation.

For dynamic tests, MTS BIONIX machine with $25\ kN$ capacity was used. For strain rates $0.1\ s^{-1}$ and $10\ s^{-1}$ velocities are adjusted to $0.5\ mm/s$ and $50\ mm/s$, respectively. During experiments, $2D$ strain fields are captured using high speed camera Phantom with a 1 megapixel camera. As it is shown in the Figure 1 (b), $5\ mm$ is chosen as the initial length of extensometer. Figure 2 (a) shows the engineering stress- strain curves at different strain rates. As can be seen in the figure, an increase of yield stress for different strain rates display the expected behaviour and the strain rate sensitivity of the material is clear. The extensions at strain rates $0.1\ s^{-1}$ and $10\ s^{-1}$ are bigger than static one, since the geometry is different and the initial length is pretty smaller as well. The strain rate sensitivity m, has to be calculated in terms of true stress and strain values and the range of 0.03 to 0.2 true strain is chosen for m profile determination. Figure 2 (b) indicates the true stress- strain curves for those strain rates.

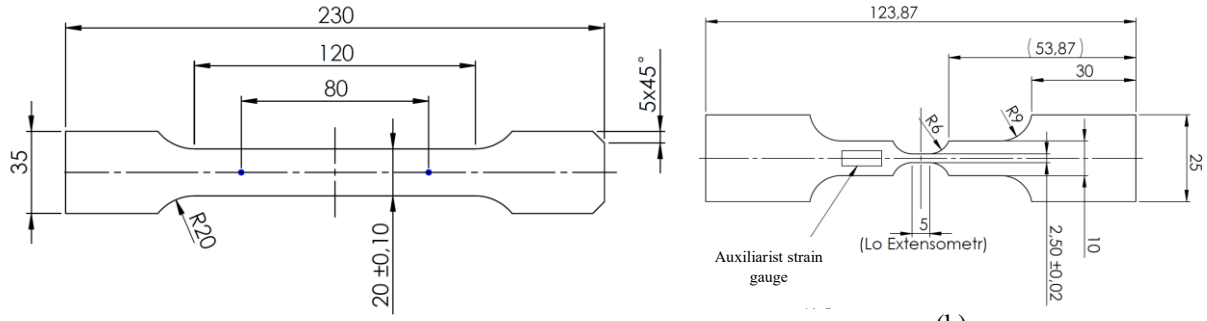

(a) (b)

Figure 1: (a) standard dog-bone sample for static test (b) Geometry of tensile sample for dynamic test

m Profile is determined by plotting true logarithmic stress versus true logarithmic strain at given true strain values and it is shown in the Figure 2 (c). As can be seen in the figure and according to Equation (1), m is the gradient of linear regression of all points with the same true strain value and resulting m-profile obtained from tensile test is depicted in Figure 2 (d). Therefore, yield curves at aforementioned range of the true strain play an active role of the resulting m profile. As it is shown in Figure 2 (d), strain rate sensitivity decreases with

increasing the true strain level.

For static test, the flow curve is extrapolated using Abaqus FEM based software for numerical simulation with conventional plasticity [18] based on von Mises material. As it was mentioned above, standard dog-bone in Figure 1 (a) was used for numerical simulation. Mesh sizes in the centre of specimen was $0.8\,mm$ and in surrounding area was $1.2\,mm$.with 4 C3D8R elements (according to Abaqus library) along the thickness. Flow curve in Figure 3 (a), is extrapolated using El-Magd hardening law (Equation (2)) and it is calibrated through inverse analysis by comparing numerical and experimental force-displacement curves. Figure 3 (b) compares the numerical and experimental force- displacement curves. As can be seen in the figure, a close agreement is achieved between numerical and experimental results and it proves the appropriate extrapolation of the flow curve. Calibrated parameters for El- Magd hardening law are summarized in Table 2. In next section, stack compression experiment is designed thanks to the characterized parameters from tensile tests.

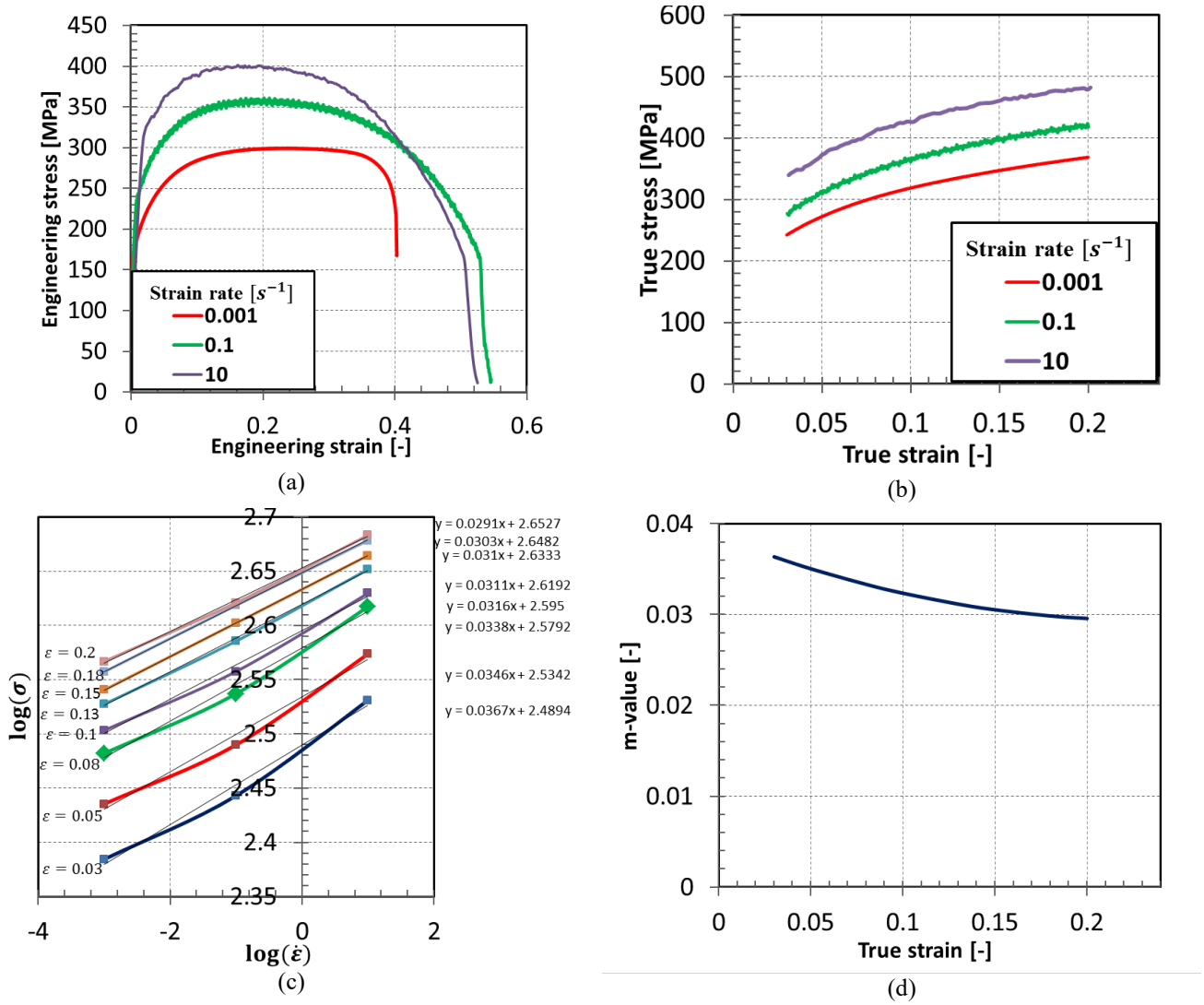

Figure 2: (a) Engineering stress- strain curves (b) True stress- strain curves at interested range (c) Logarithmic stress-strain rate space for m-value determination (d) m profile

$$\sigma_0(\varepsilon) = c_1 + c_2\varepsilon + c_3[1 - e^{-c_4\varepsilon}] \quad (2)$$

Table 2: Calibrated parameters of El-Magd hardening law

c_1	c_2	c_3	c_4
172	375	112	24

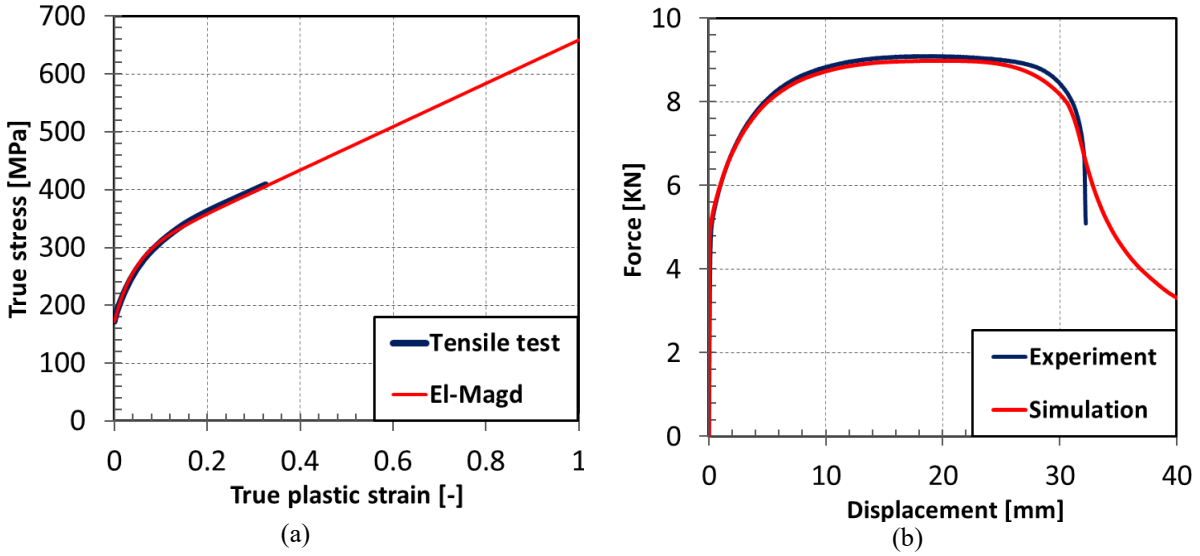

(a) (b)

Figure 3: (a) Extrapolation of the flow curve (b) Experimental and numerical force-displacement curves

2.2 Stack compression discs

2.2.1 Experiment design using numerical simulation

In this section, the experiment is designed in order to achieve highest deformation with as low as possible friction effects. In this experiment, a set of stacked discs must be available at which discs are arranged in a tool to obtain a correct alignment between the discs. The ratio of height (H) to diameter (D) should be smaller than 1.5 for stability of the stacked discs. Moreover, the machine load capacity must be taken into account. Therefore, two types of discs with diameters 15 mm and 12 mm are chosen for numerical simulation. The former diameter is simulated with 9 layers while the latter with 13 layers. As it was mentioned above the sheet thickness is 1.5 mm. For the first case of numerical simulation with 15 mm diameter and 9 layers satisfies the stability constrain ($\frac{H}{D} \leq 1.5$), whereas for the second case the ratio a little bit exceeded the limit, but it is not crucial for the real experiment. It is worth noting that the friction effect in the middle layer is the lowest and the goal of the real experiment is to capture the deformation in the middle layer during the experiment using DIC system. Therefore, the number of layers should be odd number.

For stack compression tests, two pairs of DIC system are required to capture deformations in rolling and transversal directions. Merklein and Kuppert [6] proposed a formula for measuring of the real area of the circular discs during the experiment using major strains in each pair of DIC system. Equation (3) provides the real area during stack compression test at which ε_1 and ε_2 are the principal strains in rolling and transversal directions, respectively:

$$A = \left(\left(\frac{e^{\varepsilon_1} + e^{\varepsilon_2}}{2} \right) \frac{D}{2} \right)^2 . \pi \tag{3}$$

For numerical simulations, it is assumed that friction coefficients between plate-disc and disc-disc are considered 0.115 and 0.20, respectively. Figures 4 (a) and (b) show the Mises stress contour of deformation for diameters 15 mm and 12 mm in the half cut view almost at the same level of deformation, respectively. As can be seen in the figures, the Mises stress distribution is more uniform in Figure 4 (b) with 13 layers. Force-displacement curves are presented in Figure 4 (c) in order to evaluate the maximum load level required for the real experiment. As can be seen in the Figure 4 (c), force amplitude can be significantly reduced by reducing the disc diameter. The true area is calculated according to Equation (3) in the middle layer, i.e. 5th and 7th layers, respectively. Afterwards, true stress can be obtained from division of the force to the true area. Subsequently, elastic parts are removed and true plastic stress- strain curves for both curves are depicted in Figure 4 (d) and compared with extrapolated flow curve in section 2.1. In Figure 4 (d), it is obvious that experiments on 13 layers discs with 12 mm diameter can provide more convenient result with wider range of true plastic strain, however, it is worth noting that the alignment of the stacked discs in practice can become more difficult by reducing the diameter.

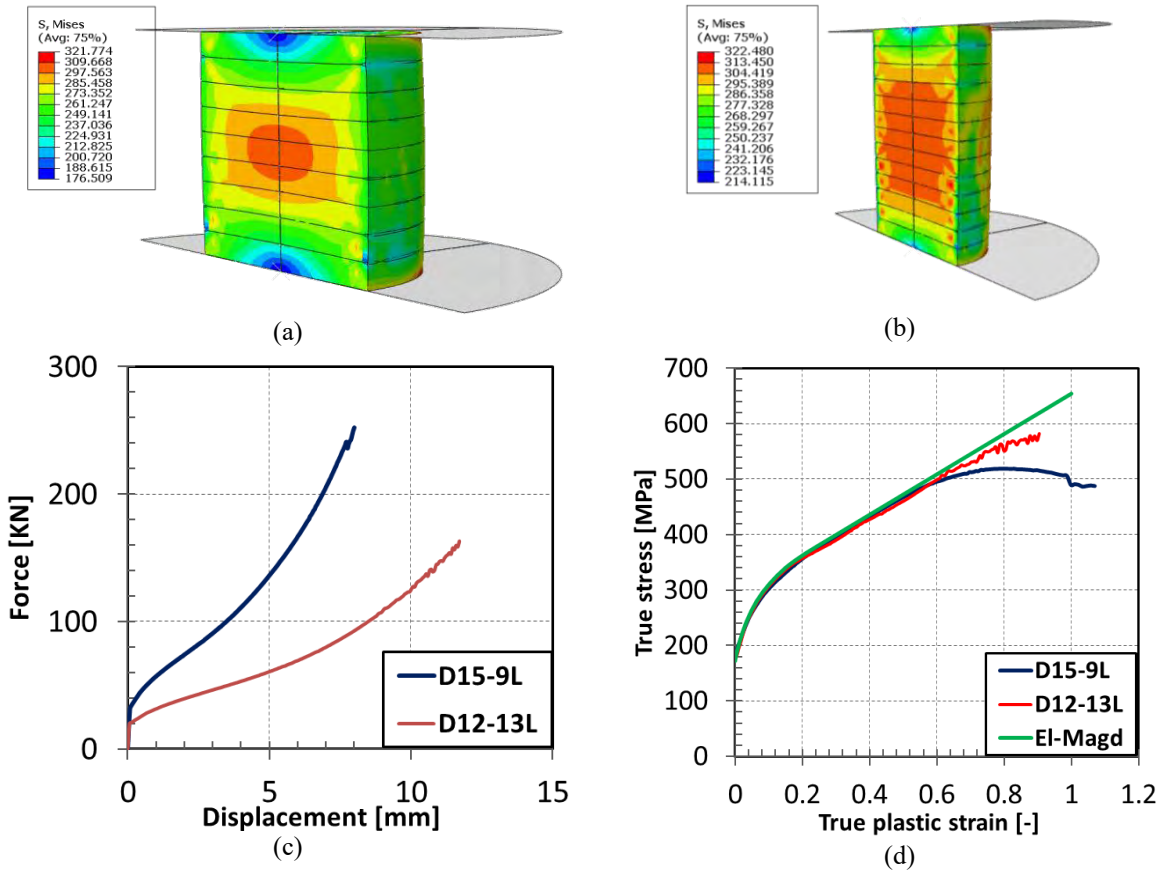

Figure 4: (a) Contour of Mises stress on 9 layers stacked discs with diameter 15 mm (b) Contour of Mises stress on 9 layers stacked discs with diameter 15 mm (c) Comparison of force- displacement curves (d) obtained numerical flow curves and comparison with El-Magd curve

2.2.2 Experimental setup

According to the obtained numerical results in Figure 4, 13 layers with 12 mm diameter are stacked and arranged to obtain a correct alignment. As it was mentioned above, two pairs of GOM Aramis^{TM} DIC systems with 12 and 4 megapixels are utilized to monitor $3D$ strain fields during the experiment in rolling and transversal directions, respectively. Figure 5 (a) represents the experimental setup. Experiments were conducted at different strain rates 0.001 s^{-1}, 0.1 s^{-1} and 10 s^{-1} which are corresponding to the velocities 0.013 $^{mm}/_{s}$, 1.5 $^{mm}/_{s}$ and 13.82 $^{mm}/_{s}$, respectively. For each strain rate three experiments were performed. For strain rate 10 s^{-1}, two pairs of high speed Phantom cameras with 1 megapixel resolution were used; however, the results were not acceptable due to the low resolutions of the cameras. Thus, material behaviour at strain rate 10 s^{-1} is excluded for stack compression test. For strain rates 0.001 s^{-1} and 0.1 s^{-1} frequency was adjusted to 1 Hz and 50 Hz, respectively. Discs are glued together for better stability and it is quite useful, especially for high strain rate experiments in which initial machine impact on stacked discs can cause eliminate the alignment. As it was mentioned, the true area is calculated using Equation (3) and Figure 5 (b) shows true stress- strain curves for those strain rates. As can be seen in Figure 5 (b), the range of 0.08 to 0.6 true strains is chosen for m profile determination. Similar to uniaxial tensile test in Section 2.1, m profile is the gradient of linear regression of all points with the same true strain value and it is illustrated in Figure 5 (c).

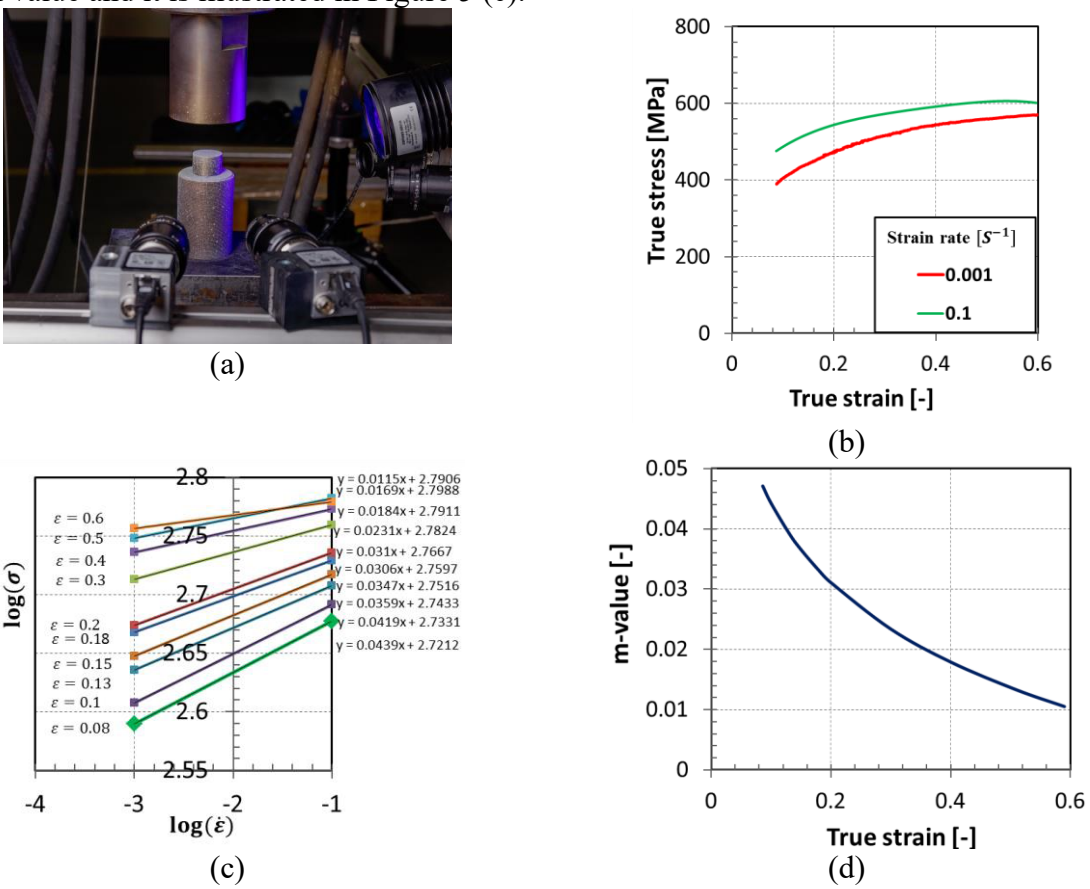

Figure 5: (a) Experimental setup (b) True stress- strain curves at interested range (c) Logarithmic stress- strain rate space for m-value determination (d) m profile

Finally, Figure 5 (d) represents obtained m profile from stack compression test. It is obvious in Figure 5 (d) that the material strain rate sensitivity is decreasing with increasing the deformation level and similar result was observed from uniaxial results (Figure 3 (d)).

3 MATERIAL HARDENING INTEGRATED WITH STRAIN RATE SENSITIVITY

Strain rate sensitivity has a significant influence on the material behaviour, especially during forming simulations. Therefore, the obtained m profiles from uniaxial tensile and stack compression tests can be integrated in the material hardening model. Work hardening was presented in Equation (2) and Johnson-Cook (J-C) model for strain rate sensitivity can be utilized as well in equation (4):

$$\sigma(\varepsilon, \dot{\varepsilon}) = \sigma_0(\varepsilon).(1 + c_{J-c} ln\left(\frac{\dot{\varepsilon}}{\dot{\varepsilon}_0}\right)) \tag{4}$$

Where c_{J-c} is corresponding to the m value, $\dot{\varepsilon}$ is the strain rate and $\dot{\varepsilon}_0$ is the reference strain rate. The m-values from uniaxial tensile and stack compression tests which were already presented above in Figures 2 (d) and 5 (d) can be denoted by $m_{tensile}(\varepsilon)$ and $m_{stack\ test}(\varepsilon)$, respectively. Both curves are modelled using logarithmic equations and are expressed in Equation (5):

$$\begin{aligned} m_{tensile}(\varepsilon) &= A.\ln(\varepsilon) + B \\ m_{stack\ test}(\varepsilon) &= C.\ln(\varepsilon) + D \end{aligned} \tag{5}$$

Table 3 summarizes the coefficient values in Equation (5). Finally, m-values from Equation (5) can be combined into one equation. Equation (6) takes into account work flow and strain rate sensitivity from tensile and stack tests.

Table 3: Coefficients of logarithmic equations

Tensile test		Stack compression test	
A	B	C	D
-0.0399	0.0369	-0.0190	0.0005

$$\begin{aligned} \sigma\left(\varepsilon, \dot{\varepsilon}, \frac{\sigma_2}{\sigma_1}\right) = \sigma_0(\varepsilon).\Bigg[\left(1 - \frac{\sigma_2}{\sigma_1}\right).\left(1 + (A.\ln(\varepsilon) + B).ln\left(\frac{\dot{\varepsilon}}{\dot{\varepsilon}_0}\right)\right) \\ + \left(\frac{\sigma_2}{\sigma_1}\right).\left(1 + (C.\ln(\varepsilon) + D).ln\left(\frac{\dot{\varepsilon}}{\dot{\varepsilon}_0}\right)\right)\Bigg] \end{aligned} \tag{6}$$

Where σ_1 and σ_2 are the principal stresses. Equation (6) describes the material hardening depending on true strain, strain rate and loading condition with consideration of $0 < \varepsilon \leq 0.6$. It is clear that for uniaxial tensile $\sigma_2 = 0$ and for equi-biaxial $\sigma_1 = \sigma_2$, therefore, Equation (6) can be reduced according to the loading condition to the relevant form.

4 CONCLUSIONS AND FUTURE RESEARCH

In this work, strain rate sensitivity of mild ferritic steel DC01 was investigated under uniaxial tensile and stack compression tests. Uniaxial tensile tests were performed at different strain rates and m profile was discovered, however, at low strain level. In order to observe the material strain rate sensitivity at higher level of deformation, stack compression test was used as an alternative for Bulge test in the present work. First, stack compression test was designed

thanks to the numerical simulation to specify the number of layers, disc's diameter and force amplitude. It was observed that experiment with 13 layers and 12 *mm* disc's diameter can provide uniform deformation along the stacked disc's height. Therefore, stack compression experiments were conducted at different strain rates. Similar to uniaxial tensile test, m profile was obtained, but at higher strain level and it was observed that for both experiments, material strain rate sensitivity decreases with increasing the deformation level. Finally, strain rate sensitivity profiles from both tests, were integrated with material hardening.

In this work, the constant velocity was applied to the stacked discs during the experiment. However, the strain rate during experiment had a little variation. Therefore, for further investigations, the authors would like to impose the velocity profile to keep strain rate constant during the experiment.

ACKNOWLEDGEMENTS

This paper is a result of the project Development of West-Bohemian Centre of Materials and Metallurgy No.: LO1412, financed by the MEYS of the Czech Republic and project methods development for formability assessment of thin sheets considering anisotropy and non-linear loading path No.: TF02000072, financed by Technology Agency of the Czech Republic.

REFERENCES

[1] Jocham, D., Norz, R., & Volk, W. (2017). Strain rate sensitivity of DC06 for high strains under biaxial stress in hydraulic bulge test and under uniaxial stress in tensile test. *International Journal of Material Forming*, *10*(3), 453–461. https://doi.org/10.1007/s12289-016-1293-8

[2] ISO copyright office (2013) Metallic Materials-Sheet and strip determination of biaxial true stress-true strain curve using hydraulic bulge test with optical measurement system. ISO/DIS 16808:2013.

[3] Pawelski, O., (1967), Über das Stauchen von Hohlzylindern und seine Eignung zur Bestimmung der Formänderungsfestigkeit dünner Bleche. Archiv für Eisenhüttenwesen 38, pp. 437-442.

[4] Peters, P.R., (2015), Yield functions taking into account anisotropic effects for an improved virtual representation of deep drawing process, *Doctoral thesis ETH Zurich*.

[5] Chongthairungruang, B., Uthaisangsuk, V., Suranuntchai, S., & Jirathearanat, S. (2013). Springback prediction in sheet metal forming of high strength steels. *Materials and Design*, *50*, 253–266. https://doi.org/10.1016/j.matdes.2013.02.060

[6] Merklein, M., & Kuppert, A. (2009). A method for the layer compression test considering the anisotropic material behavior. *International Journal of Material Forming*, *2*(SUPPL. 1), 483–486. https://doi.org/10.1007/s12289-009-0592-8

[7] Suttner, S., & Merklein, M. (2016). Experimental and numerical investigation of a strain rate controlled hydraulic bulge test of sheet metal. *Journal of Materials Processing Technology*, *235*, 121–133. https://doi.org/10.1016/j.jmatprotec.2016.04.022

[8] Wagoner, R. H., & Wang, N. M. (1983). Operant strain-rate sensitivity during tensile necking. *Metallurgical Transactions A*, *14*(11), 2395–2406. https://doi.org/10.1007/BF02663315

[9] Miura, K., Takagi, S., Furukimi, O., Obara, T., & Tanimura, S. (2010). Dynamic Deformation Behavior of Steel Sheet for Automobile. In *SAE Technical Paper Series* (Vol. 1). SAE International. https://doi.org/10.4271/960019

[10] Wilson, D. V. (2013). Strain-rate sensitivity and effects of strain rate in sheet forming. *Metals Technology*, *7*(1), 282–292. https://doi.org/10.1179/030716980803287297

[11] Ghosh, A. K. (2010). The Influence of Strain Hardening and Strain-Rate Sensitivity on Sheet Metal Forming. *Journal of Engineering Materials and Technology*, *99*(3), 264. https://doi.org/10.1115/1.3443530

[12] Hosford, W.F., (2000), Effect of strain rate exponents on neck shape, *IDDRG*, pp.95-99.

[13] Shi, M. F., & Meuleman, D. J. (1995). On certain aspects of strain rate sensitivity of sheet metals. *Journal of Materials Engineering and Performance*, *4*(3), 321–333. https://doi.org/10.1007/BF02649070

[14] Schindler, I., Hadasik, E., & Kawalla, R. (2016). Strain-Rate Sensitivity in Hot Forming of Steels - Influence of Microstructure, Temperature and Chemical Composition. *Steel Research International*, *74*(10), 617–623. https://doi.org/10.1002/srin.200300241

[15] Farahnak, P., Urbanek, M., & Džugan, J. (2017). Investigation Study on Determination of Fracture Strain and Fractuer Forming Limit Curve Using Different Experimental and Numerical Methods. In *Journal of Physics: Conference Series* (Vol. 896). Institute of Physics Publishing. https://doi.org/10.1088/1742-6596/896/1/012082

[16] Farahnak, P., Prantl, A., Dzugan, J., Konopik, P., & Prochazka, R. (2017). Sheet necking prediction in forming limit diagrams with the anisotropy influence incorporation. In *IOP Conference Series: Materials Science and Engineering* (Vol. 179). Institute of Physics Publishing. https://doi.org/10.1088/1757-899X/179/1/012023

[17] Farahnak, P., Konopik, P., Rund, M., Džugan, J., & Rzepa, S. (2018). Applicability of miniature tensile test in the automotive sector. In *IOP Conference Series: Materials Science and Engineering* (Vol. 461). Institute of Physics Publishing. https://doi.org/10.1088/1757-899X/461/1/012043

[18] Viera, A.F.C. (2017). Material Modelling: Applications, Challenges and Research. *ISBN: 9781536121612. Nova Science Publishers. New York, Chapter 8: The Numerical Non-Linear Analysis of Elastoplastic Materials Using the Radial Point Interpolation Method.*